Multiscale prediction of acoustic properties for glass wools: computational study and experimental validation

Mu He, Camille Perrot, Johann Guilleminot, Pierre Leroy, Gary Jacqus

inter.noise
27-30 AUGUST HONG KONG 2017

Multiscale prediction of acoustic properties for glass wools: computational study and experimental validation

Mu HE[1], Camille PERROT[1], Johann GUILLEMINOT[1]; Pierre LEROY[2]; Gary JACQUS[3]

[1] Multi-Scale Modeling and Simulation Laboratory, University of Paris-Est Marne-la-Vallée, France

[2] Isover Saint-Gobain CRIR, B.P. 10019, 60291 Rantigny Cedex, France

[3] CSTB, 84 Avenue Jean Jaures, Champs-sur-Marne, 77447 Marne-la-Vallée Cedex 2, France

ABSTRACT

This work is concerned with the multiscale prediction of the transport properties associated with industrial glass wool samples. In a first step, an experimental characterization is performed on various products using optical granulometry and porosity measurements. A morphological analysis, based on scanning electron imaging, is further conducted in order to identify the probability density functions associated with the fiber's angular orientation. A computational framework is subsequently proposed and allows for the reconstruction of an equivalent fibrous network. Multiscale simulations are carried out to estimate key transport properties such as the static viscous permeability and the viscous characteristic length. The results are finally compared with the experimental data and used to assess the relevance of both the reconstruction procedures and the multiscale computations.

Keywords: fibrous materials, micro-macro. I-INCE Classification of Subjects Number(s): 23, 35, 51, 76.

1. INTRODUCTION

Diffusion and fluid flow in random fibrous media are encountered in many processes of great interest, such as filtration, composite fabrication, and sound insulation. Here we are concerned with a better understanding of the transport processes through fibrous acoustic materials in order to predict the acoustical properties of lightweight glass wool samples. The other purpose of this paper is to relate fiber structure to transport coefficients of such random fiber geometries by choosing the appropriate microstructural parameters and formulating a suitable multiscale framework.

What is the microscopic basis of macroscopic properties in acoustic fibrous media? How do macroscopic transport properties depend on the microstructural parameters of a fibrous material? These are two of the many questions that have dominated studies of fluid flow and thermal diffusion through microscopically-disordered fibrous materials such as glass wools. Such questions may be addressed in a variety of ways [1,2]. Perhaps, the most direct method is to conduct a series of laboratory measurements on samples of varying sizes and types [3-8]. Alternatively, in the quest for theoretical understanding, one may seek to better understand the mathematical or physical basis of the generalized Darcy-scale equations for macroscopic transports [9-14]. Lastly, one can consider studies based on numerical simulations [15-17].

Each of these approaches has strengths and weaknesses. Laboratory measurements are of undisputed value; however, their usefulness may be limited to a specific range of already available manufactured materials. Importantly, the attempts in the literature of fibrous materials where transport properties have been related empirically to microstructural parameters – usually through some kind of power law with fitted exponents – cannot reflect what the microphysical origins are behind exponents modifications; suggesting that this approach is not appropriate to understand transport processes in fibrous materials. Analytical studies, on the other hand, are not necessarily limited to a specific kind of fiber materials, but they usually require simplifying assumptions (e.g., periodic array of cylinders [16], specific fiber orientations [19,20], or negligible interaction between the shear stress fields of

[1]camille.perrot@u-pem.fr

neighboring fibers [21]) that have only a partial relevance to reality. Numerical simulation usually attempts to bridge the gap between theory and experiments. It is typically hampered, however, by either the need to simplify geometry [16,18] or physics [15,22]. In recent years, however, another approach to the numerical study of diffusion and fluid flow through fibrous media has gained some popularity. The idea is to numerically solve the asymptotic behaviors of the linearized Navier-Stokes and heat equations in a realistic microscopically disordered geometry, and then study how volume-averaged properties of the diffusion process and the fluid flow depend on the details of the microstructures. Such studies offer the ability to study the micro-physical basis of macroscopic transport without the need for simplified geometries or physics; they are however limited to samples of small size.

Considering the difficulties that have been stated about empirical and analytical approaches, an attempt to relate fibrous structure to transport parameters should be based on direct measurements of the microstructural parameters of a single fibrous sample. Examples of such microstructural parameters include porosity, specific surface area, and some kind of average or typical fiber diameter and fiber orientation. We could then proceed to numerically solve the appropriate transport equations in a reconstructed fibrous microstructure. A challenge is in choosing the appropriate microstructural parameters and in proposing a reconstruction procedure as a way of predicting transport properties of the sample.

This work follows a series of papers focusing on the determination of the acoustic properties of random fibrous materials from their microstructures, thus extending the earlier developed methodologies for foams to random fibrous media (see for instance Sec. 1.2 of Ref. [23] for a recent literature review on foams): **(1)** First, we examined a reconstruction methodology of a random fibrous medium that can account for the external porosity of the material, as well as fiber diameters and orientations [24]. The material under consideration was made of natural fibers and synthetic fibers used as a thermal binder. The acoustic properties were computed assuming long wavelength and rigid skeleton without any adjusted parameter. An experimental validation was provided by comparison with permeability and sound absorption measurements. Thus, the sample was relatively simple because it was made of two different populations of fibers, each of them having a constant diameter. Moreover, the fibers were long when compared to the size of the reconstructed representative elementary volume. In particular, this study indicates that the considered case consists in a model material that showed a sharply peaked distribution, both in the diameters and the lengths of the fibers. **(2)** Secondly, we addressed the question of whether a fibrous medium made of a non-sharply peaked distribution of fiber diameters can be represented by an equivalent monodisperse fibrous medium with a mean fiber diameter [17]. Again, this numerical study was restricted to a sharply peaked distribution of fiber lengths.

This article focuses on fibrous media with highly complex structures: glass wools. These random fibrous media present at the same time a non-sharply peaked distribution of fibers diameters, fibers lengths, and angular orientations, making it more difficult for engineers and researchers to understand and model transport processes in acoustical fibrous materials. Therefore, our approach to model the acoustical properties of random fibrous media by means of a multi-scale method differs from the numerical models in the literature (it should be noticed at this point that the determination of the elastic properties of random fibrous media from their microstructural characteristics is out of the scope of this paper). Indeed, although several numerical studies of some of the microstructural features that are at play in a non-woven acoustical material have been proposed, they have described only the viscous fluid flow [15], sometimes adding visco-thermal coupling but it was limited to two-dimensional microstructures [16], or investigated the effect of fiber diameter and fiber orientation on the acoustical properties of model materials [17,24,25]. None of these studies however attempted to resolve simultaneously both the physics and the microgeometry involved in complex random fibrous samples: the non-sharply peaked distributions associated with fiber lengths, diameters and orientations; and the visco-inertial and thermal dissipation mechanisms, which correspond to transport parameters entering into the description of the acoustical macro-behavior of porous media.

This paper is organized as follows. Sec. II is devoted to the experimental characterization of the acoustical fibrous materials under study, at both micro- and macro- scales. Sec. III deals with the introduction of a stochastic model, from which all the transport properties of interest are computed and further compared with measurements. Sec. IV concludes this work.

2. Experimental Characterization of the Random Fibrous Network and Transport Properties

This section is concerned with the statistical characterization of the fibrous network associated with manufactured glass wools. The raw materials and the experimental setup are first described in Sec. 2.1. The statistical results are then presented in Sec. 2.2.

2.1 Description of the Raw Materials and Methodological Aspects

In this study, we consider glass wools manufactured using sand, limestone and soda ash, as well as recycled off-cuts as the basic raw materials. The raw materials are melted in a furnace at very high temperatures, typically between 1050 ℃ to 1500 ℃. The mixture is drawn through tiny holes in rapidly rotating spinners. This process shapes it into fibers. The structure and density of the product may be adapted according to its final usage. Small quantities of binding agents are added to the fibers. The glass wool is then hardened in a curing oven at around 200 ℃, and is cut to the required size and shape. Ten batches corresponding to different surface densities and various processing parameters are considered and labeled from 1 to 10. From a manufacturing perspective, the batches 1-5 constitute a first class of products (which will be referred to as Class 1 below) characterized by a given surface density S_1 (which is left undefined for industrial confidentiality reasons) yielding a porosity of about 0.995. Similarly, the batches 6-10 exhibit a surface density $S_2 > S_1$ (with a porosity equal to 0.985 approximately), and represent a second class of raw materials (which is denoted by Class 2). Samples of the material under consideration are shown at both the microscopic and macroscopic scales in Fig.1.

In order to proceed with the multiscale analysis, the random fibrous network is characterized by measuring key geometrical parameters, including the diameters and lengths of the fibers, as well as their orientation angles in horizontal and vertical planes (the former are planes parallel to (O, e_1, e_2), while the latter correspond to planes parallel to (O, e_2, e_3) in the coordinate system depicted in Fig. 1). More specifically, the measures for the diameters and lengths are automatically obtained by using a granulomorphometer. The fibers are taken by coring with a syringe, the maximum length of the fibers being equal to or less than 3.6mm. Samples are blown up in order to ensure that the fibers are well separated. The fibers whose length is not more than three times the diameter and the fibers emerging from the observation window are excluded from the analysis. Micrographs are then sequentially extracted and processed by an image recognition algorithm.

The horizontal and vertical orientations of the fibers are directly measured, inside a given plane, from SEM pictures. Here, it is assumed that the microstructure is reasonably homogeneous over the macroscopic domain, so that the spatial sampling does not introduce a bias. For each product, 40 pictures are extracted for each plane of interest at random locations (note that the horizontal plane corresponds the fibrous drawing plane), as shown in Fig. 2.

On average, each product is characterized by 200 angular measurements in both the horizontal and vertical planes, using the ImageJ software [26]. Below, it is assumed that the thickness of the samples is small enough to make the effect of out-of-plane fibers negligible in the (two-dimensional) reconstruction of the microstructure.

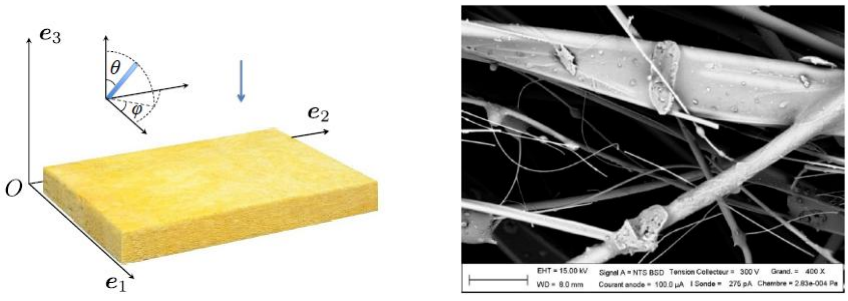

Fig. 1. This figure shows a macroscopic view of a glass wool (left panel) and the associated microstructure obtained with a Scanning Electron Microscope (SEM; right panel), for the surface density S_1. The descendent arrow shows the airflow direction. Two angles θ and φ are also defined in this coordinate system. The heterogeneity of fiber diameters can easily be observed in the micrograph. The scale bar in the SEM image is $5 \times m_D$, where m_D is the mean diameter of the analyzed fibers.

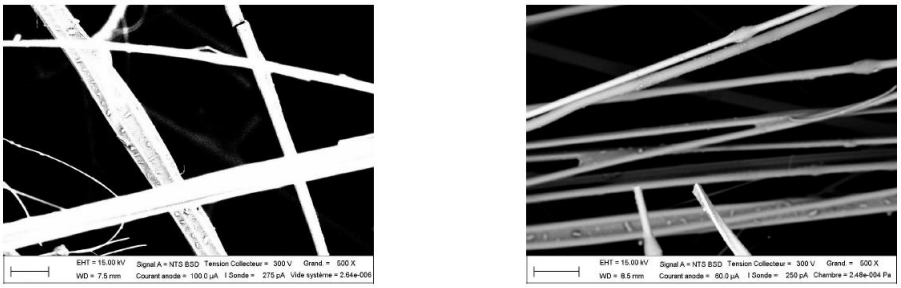

FIG. 2. Examples of micrographs taken in the horizontal (left panel) and vertical (right panel) planes. The scale bar in the SEM images is 5 $\times m_D$, in which m_D is the mean value of diameter. Sample sizes are respectively equal to $48.4m_D \times 32.5m_D$ (left) and $41.5m_D \times 27.8m_D$ (right).

2.2 Statistical Characterization of the Random Microstructure

From a statistical point of view, the probability density functions of interest are estimated through a nonparametric kernel method. The density functions associated with the diameter and length of the fibers are shown in Figs. 3 and 4 for the batches 1 and 6, respectively. In these figures, the closest fits obtained with Gamma laws are also shown (maximum likelihood estimation). It should be noticed that the fiber lengths may be underestimated due to the characterization process. For latter use, introduce the mean weighted diameter D_w defined as

$$D_w = \frac{1}{\sum_{i=1}^{N_f} V_i} \sum_{i=1}^{N_f} V_i D_i \qquad (1)$$

where V_i and D_i are the volume and diameter associated with the i-th fiber. The probability density functions of the horizontal and vertical orientation angles are shown in Figs. 5 and 6, respectively. By convention, the support of the aforementioned probability density function is defined as [0 °, 180 °].

Based on these figures, the following modeling assumptions are formulated:

- the horizontal angle φ follows a uniform distribution between 0° and 180°;
- the probability density function of the vertical angle θ provides information that corresponds to a preferred out-of-plane orientation generated by the manufacturing technique;
- the fiber diameter is distributed according to a Gamma distribution with shape parameter $1/(\delta_D)^2$ scale parameter $m_D(\delta_D)^2$, where m_D and δ_D are the mean and coefficient of variation of the diameter, respectively.These assumptions will be used in Sec. 3 in order to define the geometry of the fibrous media within the multiscale framework.

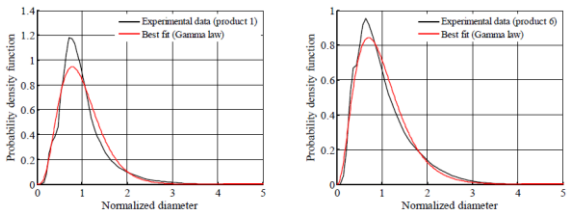

FIG. 3. The estimated probability density function of fiber diameter is shown for products 1 (left panel) and 6 (right panel). Here, the diameter is normalized by its mean value (for confidentiality reasons).

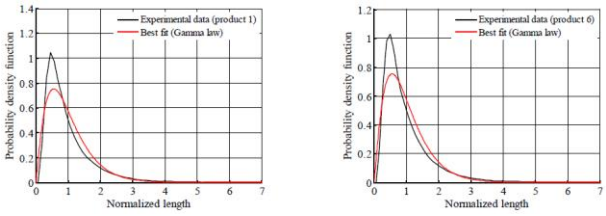

FIG. 4. The estimated probability density function of fiber length is shown for products 1 (left panel) and 6 (right panel). Here, the length is normalized by its mean value.

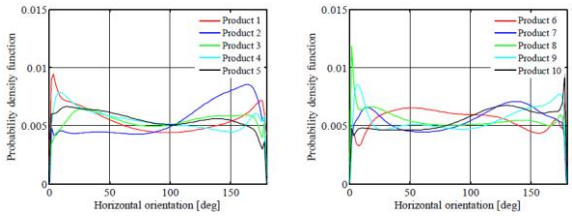

FIG. 5. The estimated probability density function of the horizontal orientation angle φ is shown for Class 1 (left panel) and 2 (right panel).

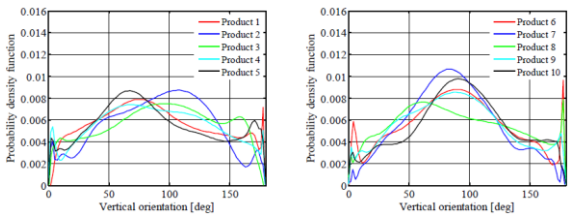

FIG. 6. The estimated probability density function of the vertical orientation angle θ is shown for Class 1 (left panel) and 2 (right panel).

2.3 Experimental Characterization of Transport Properties

The macroscopic density ρ, the porosity ϕ and the through-thickness permeability (along e_3) are determined from direct measurements [27,28]. A geometrical estimate of the thermal characteristic length Λ' can also be obtained from the knowledge of the porosity ϕ and the specific surface area S_p, since S_p is a direct output of the granulomorphometry analysis (see Eq.(6)). More specifically, the through-thickness permeability of each sample is measured for various static airflows (between 95 and 165 cubic centimeters/minute) and its quasi-static value is considered as the interpolated value for airflow equal to 0.5 mm/s. The tortuosity α_∞, the viscous characteristic length Λ, the static thermal permeability k', and the thermal characteristic lengths Λ' are determined using the indirect characterization method proposed in [29,30]. This requires, in particular, the measurement of both the equivalent dynamic bulk modulus and dynamic density, which is performed here by using the 3-microphone impedance tube method (see [31] for methodological aspects, as well as [32] for an application to foams and fibrous materials). In this study, the tube used for the measurements has a 40 mm inner diameter and the loudspeaker at one end generates a broadband random signal in the frequency band 200-4000 Hz. The determination of the aforementioned parameters is considered satisfactory when both the measured equivalent dynamic bulk modulus and equivalent dynamic density of the materials are correctly predicted [29,30].

3. Multi-scale analysis and experimental validation

3.1 Overview of the Modeling Methodology

Let Ω be the representative volume element (RVE) under consideration (with boundary $\partial\Omega$), and let Ω_f denote the part of Ω occupied by the fluid phase (the viscosity of which is denoted by η). Let $\partial\Omega_f$ be the contact surface between the fluid and solid phases. We further introduce the following notations.

Table 1 – List of symbols

Symbols	Property	Symbols	Property
ϕ	Porosity	α_∞	High-frequency tortuosity
[K]	Static viscous permeability	Λ	Viscous characteristic length
k'	Static thermal permeability	Λ'	Thermal characteristic length

3.2 Definition of the Microstructure and Multiscale Simulations

3.2.1 Definition of the Porosity and Thermal Characteristic Length

The porosity ϕ and the thermal characteristic length Λ' are purely geometrical quantities that can be readily deduced from the definition of the microstructure. More precisely, the porosity is defined as

$$\phi = V_f/V_T \tag{5}$$

where $V_f = |\Omega_f|$ is the volume occupied by the fluid (air) and $V_T = |\Omega|$ is the total volume of the domain under consideration. The thermal characteristic length Λ' is given by

$$\Lambda' = 2\phi/S_p = 2V_f/S_{fs} \tag{6}$$

in which S_{fs} is the contact area between the fluid and the solid, and $S_p = S_{fs}/V_T$ denotes the specific surface area.

3.2.2 Computational Homogenization

First of all, multiscale predictions of the static viscous permeability tensor are obtained. For this purpose, recall that the velocity **v** and the pressure p of the (incompressible) fluid satisfy the momentum equation and the mass conservation equation

$$\eta\Delta\mathbf{v} - \boldsymbol{\nabla}p = -\mathbf{G} \tag{7}$$

$$\boldsymbol{\nabla}.\mathbf{v} = 0 \tag{8}$$

in Ω_f, where **G** is a source term and the symbol "." denotes the classical inner product in $\mathbf{R}^3$. The above system of Stokes equations is supplemented with the boundary condition

$$\mathbf{v} = \mathbf{0} \tag{9}$$

on $\partial\Omega_f$, with (**v**,p) periodic on $\partial\Omega$. The components of the static viscous permeability tensor [K] can then be calculated as

$$[K]_{ij} = \phi\langle[K^*]_{ij}\rangle, \qquad 1 \le i,j \le 3 \tag{10}$$

where <.> denotes volume averaging in the fluid phase, *viz.*

$$\langle . \rangle = \frac{1}{|\Omega_f|} \int_{\Omega_f} . \, dV, \tag{11}$$

and [K*] is such that

$$v_i = -\frac{[K^*]_{ij}}{\eta} G_j \, . \tag{12}$$

In practice, three independent problems must be solved for defining the entries of [K*], each problem being defined by considering the source term $\mathbf{G}^{(i)}$, $1 \leq i \leq 3$, such that $\mathbf{G}_j^{(i)} = \delta_{ij}$, $1 \leq j \leq 3$, with δ_{ij} the Kronecker symbol ($\delta_{ij}=1$ if i=j, 0 otherwise). In this work, the Stokes equations are solved by the finite element method. More specifically, 5-node MINI tetrahedral elements are used for the velocity field, while 4-node tetrahedral elements are used for the pressure field [35]. This P^1-bubble/P^1 formulation satisfies the Babuska-Brezzi condition [36], and was implemented within in-house Matlab routines. The code verification was carried out by addressing various benchmarks proposed elsewhere in the literature (such as [37]). In order to ensure a proper refinement near the boundary layers, the mesh generation was performed by using the commercial software COMSOL Multiphysics.

The next step involves the estimation of the high-frequency tortuosity α_∞ and viscous characteristic length Λ. These quantities of interest can be obtained by solving the following potential equations

$$\mathbf{E} = -\boldsymbol{\nabla}\Phi + \mathbf{e} \, , \qquad \boldsymbol{\nabla} . \mathbf{E} = 0 \, , \tag{13}$$

in Ω_f, where $\mathbf{E}$ is the electric field, Φ is an electric potential and $\mathbf{e}$ is a (given) input macroscopic electric field. The associated boundary conditions write

$$\mathbf{E} \cdot \mathbf{n} = 0 \tag{14}$$

on $\partial\Omega_f$, with $\mathbf{n}$ the unit vector normal to the boundary $\partial\Omega_f$, and Φ periodic on $\partial\Omega$. The through-thickness high-frequency tortuosity is then defined by considering the microscopic field $\mathbf{e}=\mathbf{e}_3$ and by letting

$$\alpha_\infty = \frac{\langle \mathbf{E} \cdot \mathbf{E} \rangle}{\langle \mathbf{E} \rangle \cdot \langle \mathbf{E} \rangle} \, . \tag{15}$$

The associated viscous characteristic length reads as

$$\Lambda = 2 \left(\int_\Omega \mathbf{E} \cdot \mathbf{E} \, dV \right) \left(\int_{\partial\Omega} \mathbf{E} \cdot \mathbf{E} \, dS \right)^{-1} \, . \tag{16}$$

Finally, the static thermal permeability $K_0^{(0)}$ is estimated by solving the heat transfer equation, namely

$$\Delta u = -1 \tag{17}$$

in Ω_f, with

$$u = 0 \tag{18}$$

on $\partial\Omega_f$ and u periodic on $\partial\Omega$. The transport parameter $k'^{(0)}$ is then obtained as

$$k'^{(0)} = \langle u \rangle \, . \tag{19}$$

The two boundary value problems that are respectively defined by Eqs. (13-14) and Eqs. (17-18) are presently solved by using 4-node tetrahedral finite elements.

3.2.3 **Definition of a Random Model**

We now introduce a random model involving the features characterized through the experiments. The model is, in part, parametrized by the angles defining the orientation of the fibers: these angles are sampled in accordance with the probability law inferred from the database. Regarding the definition of the diameters, three types of configuration are considered as follows:

- in the first random model, the diameter is randomly sampled for each fiber, according to the Gamma law estimated from the data (see Fig. 3 for instance);
- in the second model, the diameter is similarly sampled for each fiber, but the probability distribution corresponds to weighted diameters.
- in the third type of configuration, the diameter is set equal to D_w, regardless of the fiber under consideration.

Once the number of fibers has been determined, the sampling of the fiber diameter and length is performed iteratively to populate the RVE, using either a standard random generator (for labelled

distributions) or the inverse transform method with empirical distributions (for the probability law involving weighted diameters). Similarly, the orientation angles are sampled according to their empirical distributions, and the center of the fibers is sampled according to a uniform distribution. Note that the fibers are allowed to intersect, since it does affect the prediction of transport properties. In order to ensure the periodicity of the medium, fibers exiting the RVE are forced to re-enter the domain from the opposite side. The number of fibers hence generated for each product is about 100 to 200.

One realization of the random microstructure with fiber-dependent diameters and the associated FE mesh are shown in Fig. 7 for Product 2. The solution fields for one component of the velocity field and scaled concentration field are finally shown, for illustration purposes, in Fig. 8. Note that, visually, the fluid-flow paths are clearly more concentrated, and follow a more tortuous path, than do the heat diffusion field.

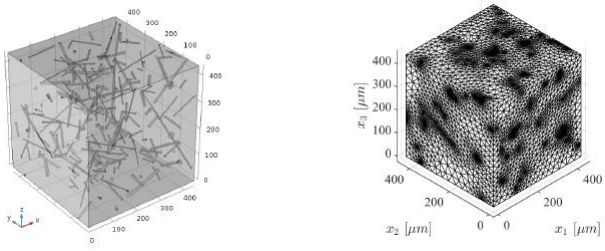

FIG. 7. Meshed view of one realization of the random microstructure associated with Product 2.

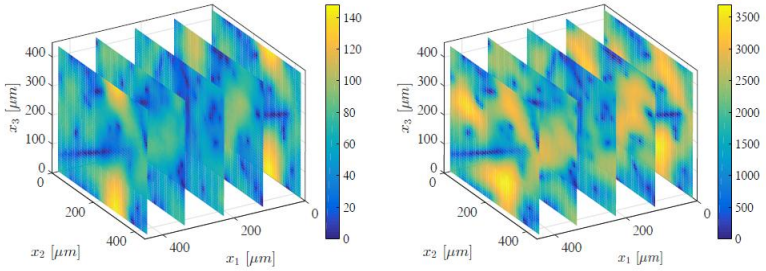

FIG. 8. Solution fields associated with the realization of the random microstructure shown in Fig. 7: velocity field $\mathbf{x}\rightarrow v_3(\mathbf{x})$ [µm/s] associated with the source term $\mathbf{G}^{(3)}$ (left panel) and scaled concentration field $\mathbf{x}\rightarrow u(\mathbf{x})$ [μm^2] (right panel).

3.2.4 **Acoustic Properties**

The effective density $\rho_{eff}(\omega)$ and the effective bulk modulus $K_{eff}(\omega)$ of the fluid phase can be evaluated by simple analytic admissible functions [10-13] as follows:

$$\rho_{eff}(\omega) = \rho_0 \alpha_0 \left[1 + \frac{1}{\tilde{\omega}} f(\tilde{\omega})\right], \tag{20}$$

$$\frac{1}{K_{eff}(\omega)} = \frac{1}{K_a}\left\{\gamma - (\gamma - 1)\left[1 + \frac{1}{j\tilde{\omega}'} f'(\tilde{\omega}')\right]^{-1}\right\}, \tag{21}$$

where ρ_0 is the air density at rest, K_a is the adiabatic bulk modulus of air and γ is its specific heat ratio. The quantities $\tilde{\omega}$ and $\tilde{\omega}'$ are dimensionless viscous and thermal angular frequencies given by the following expressions:

$$\tilde{\omega} = \frac{\omega}{\nu}\frac{K_{33}\alpha_\infty}{\phi}, \tag{22}$$

$$\tilde{\omega}' = \frac{\omega}{\nu'}\frac{k'}{\phi}, \tag{23}$$

with $\nu'=\nu/P_r$, ν being the kinematic viscosity and P_r is the Prandtl number (≈0.71 for air). $f(\tilde{\omega})$ and $f'(\tilde{\omega}')$ are shape functions defined by

$$f(\tilde{\omega}) = 1 - P + P\sqrt{1 + \frac{M}{2P^2}j\tilde{\omega}}\,, \tag{24}$$

$$f'(\tilde{\omega}') = 1 - P' + P'\sqrt{1 + \frac{M'}{2P'^2}j\tilde{\omega}'}\,. \tag{25}$$

The quantities M, M', P, and P' are referred to as dimensionless shape factors determined from

$$M = \frac{8K_{33}\alpha_\infty}{\Lambda^2\phi}, \tag{26}$$

$$M' = \frac{8k'}{\Lambda'^2\phi}, \tag{27}$$

$$P = \frac{M}{4(\frac{\alpha_{033}}{\alpha_\infty} - 1)}\,, \tag{28}$$

$$P' = \frac{M'}{4(\alpha_0' - 1)}\,. \tag{29}$$

- For P=P'=1, the dynamic response functions reduce to a 6 parameters model (ϕ, K_{33}, k', α_∞, Λ, Λ'), known as the "Johnson-Champoux-Allard-Lafarge" (JCAL) or "Johnson-Lafarge" model [10,11,13].
- A complete model relies on 8 parameters (ϕ, K_{33}, k', α_∞, Λ, Λ', α_{033}, α_0'). This is the refined "Johnson-Champoux-Allard-Pride-Lafarge" (JCAPL) model

The $\rho_{eq}(\omega)=\rho_{eff}(\omega)/\phi$ and $K_{eq}(\omega)=K_{eff}(\omega)/\phi$ are the equivalent density and bulk modulus of the so-called rigid-frame equivalent-fluid medium. Assuming plane wave solutions varying as $\exp[j(\omega t-q_{eq}(\omega)x]$, where $q_{eq}(\omega)$ represents the wave number of the equivalent fluid medium, $\rho_{eq}(\omega)$ and $K_{eq}(\omega)$ can be used to calculate the wave number and the characteristic impedance of the equivalent fluid medium with:

$$q_{eq} = \omega\sqrt{\frac{\rho_{eq}(\omega)}{K_{eq}(\omega)}}\,, \tag{30}$$

$$Z_{eq} = \omega\sqrt{\rho_{eq}(\omega)K_{eq}(\omega)} \tag{31}$$

The sound absorption coefficient at normal incidence of a porous material layer of thickness L_s backed by a rigid wall is evaluated by

$$\alpha = 1 - \left|\frac{Z_n - 1}{Z_n + 1}\right|^2\,, \tag{32}$$

with

$$Z_n = -j\frac{Z_{eq}}{Z_0}\cot(q_{eq}L_s)\,. \tag{33}$$

the effective normal impedance on the free face of the excited material, where Z_0 is the characteristic impedance of ambient air. Therefore, an estimation of the acoustic properties of fibrous media can be obtained on the basis of macroscopic parameters determined from the computational homogenization framework.

3.3 Comparison with Experimental Results

We present in Figs. 9 and 10 a comparison between the computational and experimental results for the transport parameters. We see that a quantitative appreciation of the static viscous permeability K_{33} can be obtained from both the equivalent and the random model, when a weighting of the fiber

diameters is applied (left panel of Fig. 9). On the other hand, a single random model is such that diameters distributed to a Gamma law without the weighting of the fiber diameters corresponds to underestimated static viscous permeability. It is noteworthy that the difference between the static viscous permeabilities with diameters distributed according to a weighted Gamma law and with a constant diameter equal to D_w are insignificant. Therefore, when simulating weighted fiber diameters, a simple way to simplify the generation of the random model is to use a single constant diameter equal to D_w. Our results indicate that a weighting of the diameters in volume is required to quantitatively model the static viscous permeability of a random fibrous media when the distributions of the parameters of the fibers are broad. What is the meaning of the weighting requirement in complex random fibrous webs? If the distributions of the parameters of the fibers are sharply peaked, the overall system behavior is similar to that of the individual elements. On the other hand, if the distributions of the parameters of the fibers are broad, the fibers with the largest relative volume with respect to length and diameter dominate. That means the permeability coefficient of the overall system is expressible by defining a domain Ω of typical characteristic length L where the fiber diameters are again taken to be weighted in volume.

Our simulated values for the viscous characteristic length Λ were overestimated. For a random model with weighted diameters, the ratio between the simulated and characterized data is equal to 4.16 ± 1.63 (Right panel of Fig. 9). The right panel of Fig. 9 also shows that the calculations corresponding to the second class of products (Class 2) characterized by a higher surface density are in better agreement with measurements (the ratio was 2.93 ± 0.68 for Class 2, and 5.38 ± 1.34 for Class 1). The left panel of Fig. 10 shows that, except for Product Reference 6, the characterized values of the thermal characteristic length Λ' obtained from the acoustical and granulomorphometry method differ significantly, this ratio was equal to 3.26 ± 1.05 for the ten analyzed products. One can see, however, that in a few cases the dispersion of measurements is such that the two different characterization techniques tend to provide values in better agreement (Product reference numbers 7 and 10). Because we determined the thermal characteristic length of the models from the granulomorphometry analysis, the later values are typically the same as those reported in the direct geometrical characterization method: the thermal characteristic length variations between the models and the direct geometrical characterization are relatively small (CV = 0.14). The static thermal permeability k' with the random model including weighted diameters was presumably underestimated: the ratio between the experimental and simulated data was close to two (1.96 ± 0.57) with a weighted random model. Let us mention that because all the data corresponding to the tortuosity were very close to one, they were not shown here.

It is clear from these results that the estimates of macroscopic properties based on the weighted random model are the most reliable. This is not surprising because the estimates are computed directly from transport parameters that are related to the three-dimensional micro-geometry of the fibrous structure. By contrast, the permeability based on the non-weighted model (□, black) does not readily distinguish between sharply peaked and broad distributions of the parameters of the fibers. The permeability K_{33} and the tortuosity α_∞ incorporate visco-inertial information. Here the Λ parameter calculations follow the same trends as experimental data. It is seen from the right panel of Fig. 9 that the simulations are indeed an upper bound for the experimental estimate. Two additional

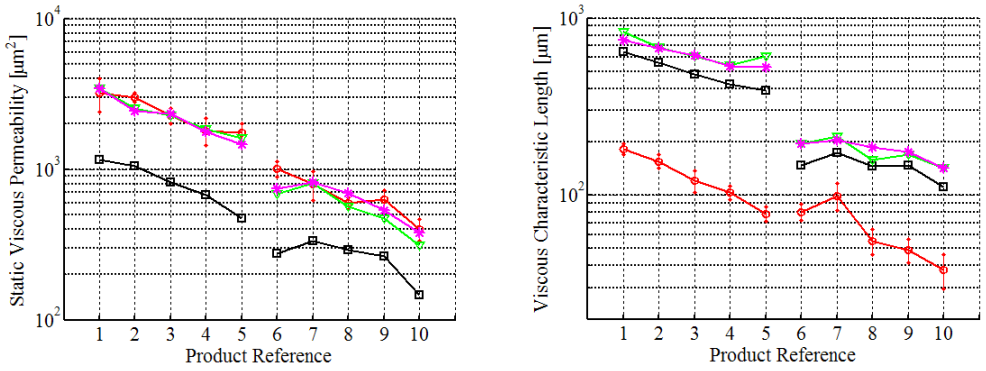

FIG. 9. Left panel: graph of the static viscous permeability. Right panel: graph of the viscous characteristic length. Colors and symbols: experimental data (○, red); random model with diameters distributed to a Gamma law (□, black); random model with distribution corresponding to weighted diameters (∇, green); random model with a constant diameter (equal to D_w) (*, magenta).

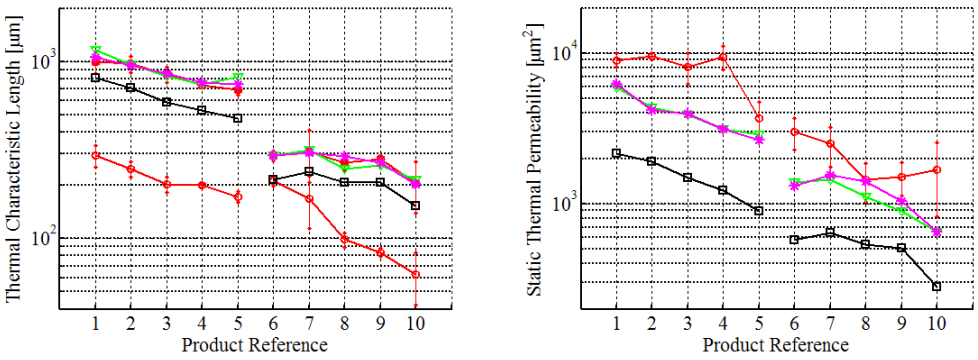

FIG. 10. Left panel: graph of the thermal characteristic length. Right panel: graph of the static thermal permeability. Colors and symbols: experimental data by characterization (○, red); experimental data with direct geometrical characterization performed using the granulomorphometer (●, red) (see Eq. 6); random model with diameters distributed to a Gamma law (□, black); random model with distribution corresponding to weighted diameters (∇, green); random model with a constant diameter (equal to D_w) (*, magenta).

points are worth making in connection with Figs. 9 and 10. Firstly, all of these macroscopic parameters were determined without any adjusted parameters. Secondly, the models considered here all depend on the morphogranulometry excluding long fibers from the analysis. Evidently, the weighting procedure implied by Eq. 17 substantially favors the smaller inter-fiber sizes. The number of fibers that was characterized is considerably smaller than that from the sample size in the experiments. As regards the overestimation of the smaller inter-fiber sizes, one can judge for oneself whether a ratio between the simulated and characterized data equals to 4.16 ± 1.63 corresponds to a half-full or half-empty glass. The same kind if remark can be drawn for the Λ' parameter, whose determination is very sensitive to ϕ since $(1-\phi)$ is very small at low densities. ($\Lambda' \sim \phi \mathbf{E}\{D^2\}/[2(1-\phi)\mathbf{E}\{D\}]$ providing that the diameters and the lengths of fibers are independent.)

In Fig. 11, we also compare the predicted and characterized sound absorption coefficients at normal incidence for the geometrical models studied here. The characterization uses the JCAL model, while the simulations results are deduced from the full JCAPL model. It is clear from these results that the experimental data are consistent with the weighted random model over the whole frequency range. It is interesting to see that the sound absorption of a glass wool can be predicted without adjustable parameters in the model for ten different products. Clearly, the difficulty in this multi-scale simulation process was the broad distribution of the parameters of the geometry.

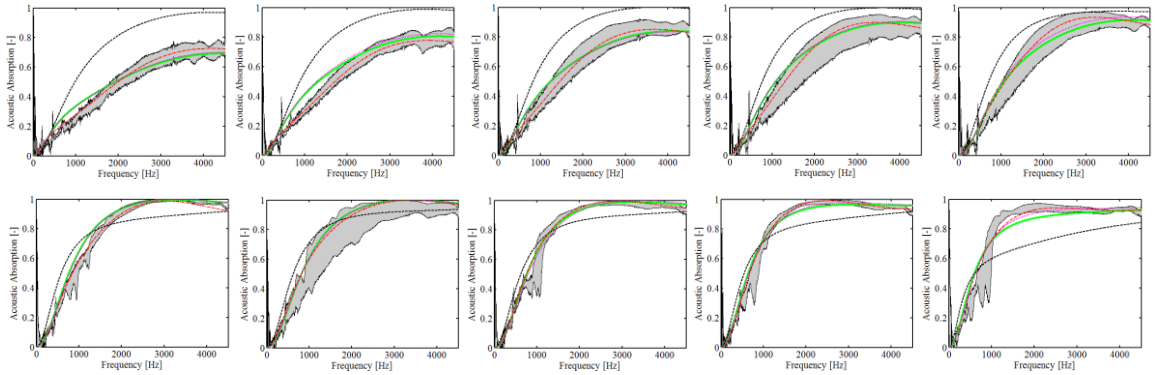

FIG. 11. Sound absorption coefficient (normal incidence). Top panel: Product 1 to 5 (from left to right). Bottom panel: Product 6 to 10 (from left to right). Colors and symbols: measurements (gray zone); inverse characterization method (dash-dot line, red); random model with diameter distributed to a Gamma law (dashed line, black); random model with distribution corresponding to weighted diameters (thick line, green); random model with a constant diameter equals to D_w (dotted line, magenta).

Finally, it should be noticed that the above (samplewise) comparison is meaningful if and only if the condition of scale separation reasonably holds for all products under consideration. Here, the fulfillment of this condition was numerically checked through numerical experiments. From a methodological standpoint, the estimation of the transport properties was first carried out on a limited set of realizations of the random microstructure (for a given product). Given the small number of virtual samples (which is typically equal to 10), the coefficients of variation associated with the predicted properties were subsequently estimated by using the maximum likelihood method with appropriate

labeled distributions. The coefficient of variation is seen to be smaller or equal to 5%, hence validating the assumption about scale separation (which can only be satisfied approximately in simulations).

4. CONCLUSIONS

The recent approach has been to treat a polydisperse fibrous media as if it was equivalent to a monodisperse fiber media, i.e. by means of an average diameter of the corresponding distribution [25]. Here, the effective fiber diameter is derived from optical granulometry and is a weighted fiber volume diameter accounting for the relative length and diameter of each fiber. Fully stochastic microstructural models were subsequently introduced in a classical manner. It was shown that the weighted random models provide an excellent estimate of the permeability K_{33}. The Λ parameter was probably the most difficult quantity to predict (and measure) accurately. Estimates of Λ were less reliable; their accuracy decreased with decreasing density. However, the sound absorption was accurately described for the 10 different glass wools under study corresponding to various processing parameters. This makes this procedure a powerful probe of the sound absorbing properties of complex fibrous materials. Moreover, in our view interesting and complementary research topics for future research lie in the multiscale determination of the tensorial elastic properties and loss factor of complex random fibrous materials (such as glass wools and rock wools).

ACKNOWLEDGEMENTS

We thank Y. Heulin and M. Daudet from Isover Saint-Gobain CRIR who performed the acoustical and morphogranulometry characterizations, respectively; and for discussions about the data analysis. P. Andrié, S. Berger, J.-B. Chéné, C. Coguenanff, E. Thibier from the thesis committee are gratefully acknowledged for providing insightful discussions and suggestions. This work was supported by the French Agency for the Environment and Energy Management (ADEME), the French Scientific and Technical Center for Building (CSTB), and the Isover Saint-Gobain Company, under the cooperative agreement ADEME TEZ14-24 with the University of Paris-Est Marne-la-Vallée.

REFERENCES

1. E. J. Garboczi, Permeability, diffusivity, and microstructural parameters: A critical review, Cem. Concr. Res. 20, 591-601 (1990).
2. P. M. Adler and J.-F. Thovert, Real porous media: Local geometry and macroscopic properties, Appl. Mech. Rev. 51, 537-585 (1998).
3. M. E. Delany and E. N. Bazley, Acoustical properties of fibrous materials, Appl. Acoust. 3, 105-116 (1970).
4. D. A. Bies and C. H. Hansen, Flow resistance information for acoustical design, Appl. Acoust. 13, 357-391 (1980).
5. Y. Miki, Acoustical properties of porous materials - modifications of Delany Bazley models, J. Acoust. Soc. Jpn. (E) 11, 19-24 (1990).
6. M. Garai and F. Pompoli, A simple empirical model of polyester fibre materials for acoustical applications, Appl. Acoust. 66, 1383-1398 (2005).
7. J. Manning and R. Panneton, Acoustical model for Shoddy-based fiber sound absorbers, Text. Res. J. 83, 1356-1370 (2013).
8. P. Kerdudou, J.-B. Chéné, G. Jacqus, C. Perrot, S. Berger, P. Leroy, A semi-empirical approach to link macroscopic parameters to microstructure of fibrous materials, in Proceedings of the 44th InterNoise (San Francisco, CA, 2015), pp. 5468-5479.
9. J. L. Auriault, L. Borne, and R. Chambon, Dynamics of porous saturated media, checking of the generalized law of Darcy, J. Acoust. Soc. Am. 77, 1641-1650 (1985).
10. D. L. Johnson, J. Koplik, R. Dashen, Theory of dynamic permeability and tortuosity in fluid-saturated porous media, J. Fluid Mech. 176, 379-402 (1987).
11. Y. Champoux, J. F. Allard., Dynamic tortuosity and bulk modulus in air-saturated porous media, J. Appl. Phys. 70, 1975-1979 (1991).
12. S. R. Pride, F. D. Morgan, A. F. Gangi., Drag forces of porous media acoustics, Phys. Rev. B 47, 4964-4978 (1993).
13. D. Lafarge, P. Lemarinier, J.-F. Allard, V. Tarnow, Dynamic compressibility of air in porous structures at audible frequencies, J. Acoust. Soc. Am. 102, 1995-2006 (1997).
14. C. Boutin, Rayleigh scattering of acoustic waves in rigid porous media, J. Acoust. Soc. Am. 122,

1888-1905 (2007).
15. K. Schladitz, S. Peters, D. Reinel-Bitzer, A. Wiegmann, J. Ohser, Design of acoustic trim based on geometric modeling and flow simulation for non-woven, Comp. Mat. Sci. 38, 56-66 (2006).
16. C. Peyrega and D. Jeulin, Estimation of acoustic properties and of the representative volume element of random fibrous media, J. Appl. Phys. 113, 104901-13 (2013).
17. H. T. Luu, R. Panneton, C. Perrot, Effective fiber diameter for modeling the acoustic properties of polydisperse fiber networks, J. Acoust. Soc. Am. 141, EL96-EL101 (2017).
18. O. Umnova, D. Tsiklauri, R. Venegas, Effect of boundary slip on the acoustical properties of microfibrous materials, J. Acoust. Soc. Am. 126, 1850-1861 (2009).
19. V. Tarnow, Compressibility of air in fibrous materials, J. Acoust. Soc. Am. 99, 3010-3017 (1996).
20. V. Tarnow, Airflow resistivity of models of fibrous acoustic materials, J. Acoust. Soc. Am. 100, 3706-3713 (1996).
21. B. P. Semeniuk and P. Goransson, Microstructure based estimation of the dynamic drag impedance of lightweight fibrous materials, J. Acoust. Soc. Am. 141, 1360-1370 (2017).
22. M. M. Tomadakis and T. J. Robertson, Viscous permeability of random fiber structures: Comparison of electrical and diffusional estimates with experimental and analytical results, J. Comp. Mat. 39, 163-188 (2005).
23. C. Perrot, Modeling of multi-scale and multi-physical properties of acoustic materials, Habilitation Thesis, Université Paris-Est, France, 2014.
24. H. T. Luu, C. Perrot, V. Monchiet, R. Panneton, Three-dimensional reconstruction of a random fibrous medium: Geometry, transport and sound absorbing properties, accepted for publication in J. Acoust. Soc. Am., Ms JASA-00503R3 (2017).
25. H. T. Luu, C. Perrot, R. Panneton, Infuence of porosity, fiber radius and fiber orientation on the transport and acoustic properties of random fiber structures, under revision in Acta Acust united Ac., Ms AAA-D-16-00177R1 (2017).
26. M. D. Abramoff, P. J. Magalhaes, S. J. Ram, Image Processing with ImageJ, Biophotonics Int. 11, 36-42 (2004).
27. Y. Salissou, R. Panneton, Pressure/mass method to measure open porosity of porous solids, J. Appl. Phys. 101, 124913-7 (2007).
28. M. R. Stinson and G. A. Daigle, Electronic system for the measurement of flow resistance, J. Acoust. Soc. Am. 83, 2422-2428 (1988).
29. R. Panneton and X. Olny, Acoustical determination of the parameters governing viscous dissipation in porous media, J. Acoust. Soc. Am. 119, 2027-2040 (2006).
30. X. Olny and R. Panneton, Acoustical determination of the parameters governing thermal dissipation in porous media, J. Acoust. Soc. Am. 123, 814-824 (2008).
31. Y. Salissou and R. Panneton, Wideband characterization of complex wave number and characteristic impedance of sound absorbers, J. Acoust. Soc. Am. 128, 2868-2876 (2010).
32. O. Doutres, Y. Salissou, N. Atalla, R. Panneton, Evaluation of the acoustic and nonacoustic properties of sound absorbing materials using a three-microphone impedance tube, Appl. Acoust. 71, 506-509 (2010).
33. L. Dormieux, D. Kondo, F.-J. Ulm, Microporomechanics (Wiley, Chichester, 2006), pp. 344.
34. J.-L. Auriault, C. Boutin, C. Geindreau, Homogenization of Coupled Phenomena in Heterogenous Media (Wiley-ISTE, London, 2009), pp. 476.
35. A. Ern and J.-L. Guermond, Theory and Practice of Finite Elements (Springer, New-York, 2004), pp. 505.
36. D. N. Arnold, F. Brezzi, M. Fortin, A stable finite element for {Stokes equations, Calcolo 21, 337-344 (1984).
37. C. Sandstrom and F. Larsson, On bounded approximations of periodicity for computational homogenization of Stokes flow in porous media, Int. J. Numer. Methods Eng. 109, 307-325 (2016).
38. J. Guilleminot, C. Soize, R. G. Ghanem, Stochastic representation for anisotropic permeability tensor random fields, Int. J. Numer. Anal. Methods Geomech. 36, 1592-1608 (2012).